14.2 STUDY OF THE ADVANCED BASELINE IMAGER (ABI) ON THE GOES-R AND BEYOND

[1]Timothy J. Schmit*, [2]Jun Li, [2]Mathew M. Gunshor, [2]Christopher C. Schmidt, [3]W. P. Menzel, [4]James Gurka, and [2]Justin Sieglaff

[1]NOAA/NESDIS, Office of Research and Applications, Advanced Satellite Products Team (ASPT)
[2]Cooperative Institute for Meteorological Satellite Studies (CIMSS), University of Wisconsin-Madison
[3]NOAA/NESDIS, Office of Research and Applications
Madison, WI 53706
[4]NOAA/NESDIS, Office of Systems Development, Silver Spring, Maryland

1. INTRODUCTION

The Advanced Baseline Imager (ABI) is being designed for future Geostationary Operational Environmental Satellites (GOES) starting with GOES-R in 2012 (Gurka and Dittberner, 2001). As with the current GOES Imager, this instrument will be used for a wide range of qualitative and quantitative weather and environmental applications. The ABI will improve over the existing GOES Imager with more spectral bands, higher spatial resolution, faster imaging, and broader spectral coverage. The ABI will improve the spatial resolution from nominally 4 to 2 km for the infrared bands and 1 to 0.5 km for the 0.6 μm band, 2 km for the 1.38 μm, and 1 km for the other visible/near-IR bands. There will be a five-fold increase of the coverage rate. The ABI expands the spectral band number to 16; five are similar to the 0.6, 4, 11, and 12 μm windows and the 6.5 μm water vapor band on the current GOES-8/11 Imagers (Table 1). For more information on the uses of the current GOES Imager; Menzel and Purdom (1994), Ellrod et al. (1998). The additional bands are a visible band at 0.47 μm for aerosol detection and visibility estimation, a visible band at 0.86 μm for the detection of aerosols and vegetation; a near-infrared band at 1.38 μm to detect very thin cirrus clouds; a snow/cloud-discriminating 1.6 μm band; the 2.26 μm will be used for particle size, vegetation and cloud properties/screening, hot spot detection, moisture determinations; mid-tropospheric bands centered at approximately 7.0 and 7.34 μm water vapor band to track atmospheric motions; an 8.5 μm band to detect volcanic dust clouds containing sulfuric acid aerosols and cloud phase; the 9.6 μm band for monitoring total column ozone; the 10.35 μm band to derive low-level moisture and cloud particle size; and a 13.3 μm band useful for determining cloud top heights and effective cloud amounts (Table 2). Table 3 summarizes improved characteristics of the ABI compared to the current GOES imager.

The six visible/near infrared bands are shown in Fig. 1 with a representative clear-sky radiance plot. These will be used to generate a number of products including visibility, vegetation, cloud cover and surface features during the day. Figure 2 shows mock spectral response functions (SRFs) of the ten bands in the infrared portion of the spectra. These mock ABI SRFs are available at: *http://cimss.ssec.wisc.edu/goes/abi/.*

* *Corresponding author address*: Timothy J. Schmit, 1225 West Dayton Street, Madison, WI 53706;
email: Tim.J.Schmit@noaa.gov.

The channel selection for ABI is a balance of heritage with existing GOES bands (on the imager or sounder), consistency with bands on other satellites (both in geostationary and polar-orbits) and the relationship between which information will be derived from the advanced high-spectral resolution sounder. Section 2 summarizes a select number of new and improved products possible with the GOES ABI. Section 3 briefly describes the uses for each of the bands on the ABI.

The weighting functions, which show the layer of observed energy for each ABI band are shown in Figure 3. These are for the standard atmosphere at a local zenith angle of 40 degrees.

2. PRODUCTS

2.1 *Imagery/Radiances*

Each of the current bands on the GOES Imager are displayed as a time-series of images. This will also be the case of each of the ABI bands. Additional information can be gleamed by differencing bands or applying principle components on the imagery (Hillger, 1996). For example, the current GOES Imager "water vapor" band 3 (6.7 μm) has many applications, ranging from estimating upper level moisture (Soden and Bretherton, 1993; Moody et al., 1999) to defining upper-level jetstreaks (Weldon et al., 1991). While the difference between the 11 and 12 μm brightness temperatures, known as the split window, helps detect dust, volcanic ash plumes, low-level moisture, and skin temperature and aids in distinguishing between cloud types and biomass burning aerosols (Ackerman, 1996; Ackerman and Chung, 1992; Moeller et al., 1996; Prata, 1989, Barton et al., 1992; Hayden et al., 1996; Prins et al., 1998). Out flow boundaries have also been observed (Dostalek et al. 1997). Also, averaged, clear-sky brightness temperatures from the imagers are being investigated for assimilating into numerical models. For example, the direct assimilation of water vapor (WV) clear-sky brightness temperatures (CSBT) from geostationary satellites became operational at ECMWF in April 2002 using the four-dimensional variational assimilation (4DVAR) system with data from METEOSAT-7. The GOES-9/10/12 CSBT products are currently being assimilated at the ECMWF. This GOES CSBT product will be improved with data from the ABI, in part due to a superior cloud mask with the additional bands and a better signal-to-noise ratio.

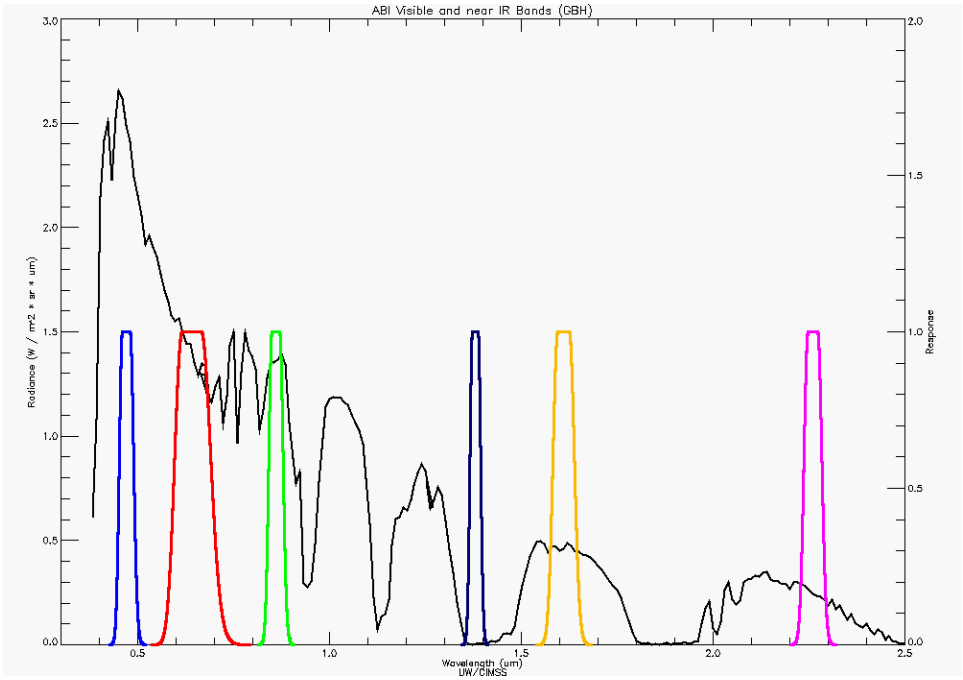

Figure 1. The spectral coverage of the six visible/near infrared bands with a representative clear-sky radiance plot. The current GOES has only one visible band (centered at approximately 0.64 μm).

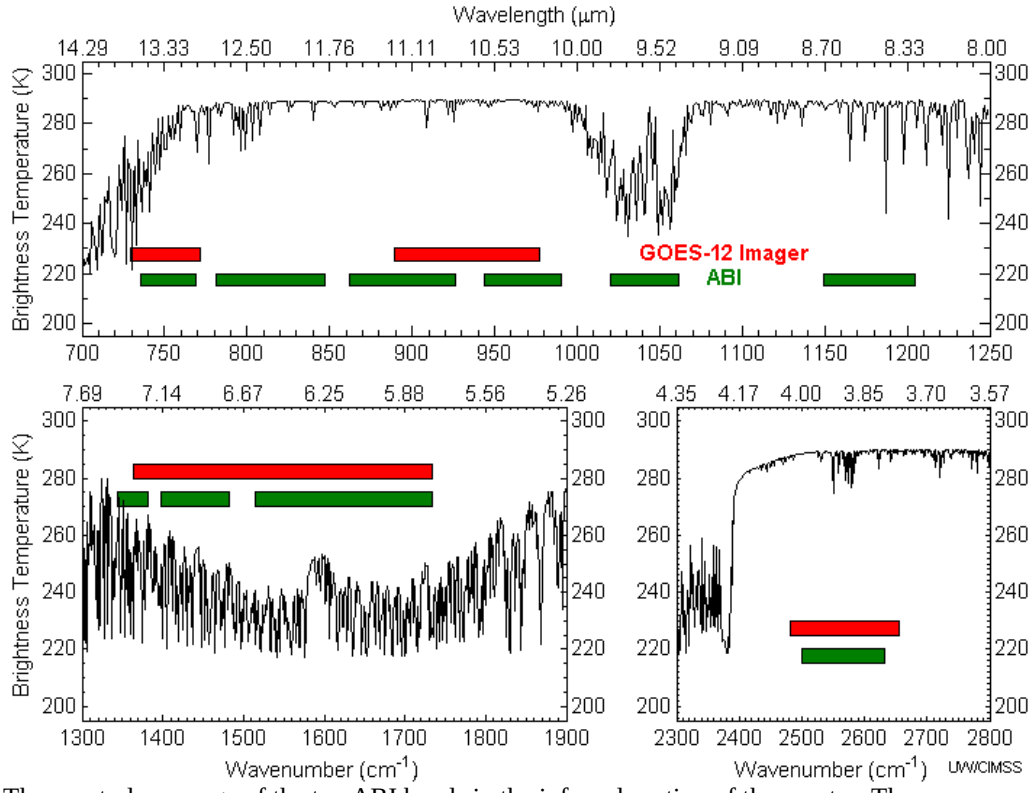

Figure 2. The spectral coverage of the ten ABI bands in the infrared portion of the spectra. These are compared with the spectral coverage from the GOES-12 imager and a sample high-spectral resolution earth-emitted spectra.

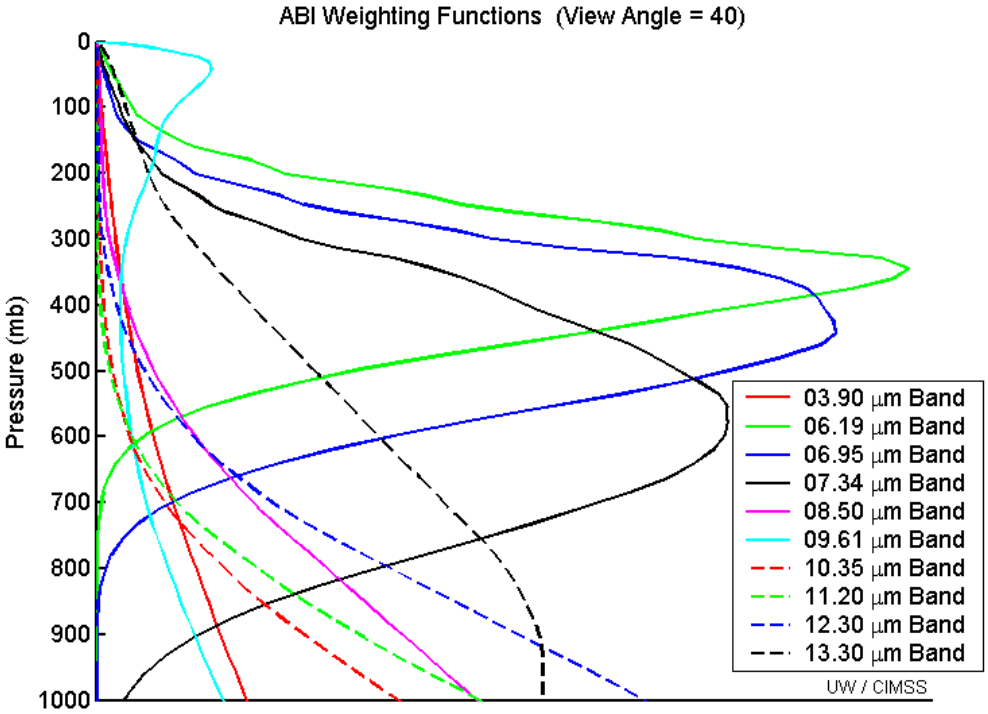

Figure 3. ABI weighting functions for the standard atmosphere at a local zenith angle of 40 degrees.

2.2 *Cloud Products*

Cloud products generated via the CO_2 absorption technique have been demonstrated from instruments on both geostationary and polar-orbiting platforms (Wylie and Wang, 1997; Schreiner et al., 1993; Wylie et al., 1994; Wylie and Menzel, 1999; Frey et al., 1999; Schreiner et al., 2001). Cloud products derived from the GOES Sounder have been used to initialize numerical models (Kim and Benjamin, 2000; Bayler et al., 2001). Improved products from the GOES ABI will include cloud top pressure (CTP), effective cloud amount (ECA) and cloud top temperature. The ECA represents the optical thickness of the cloud. Recent work has shown that the difference between the 6.7 μm and the 11 μm band is correlated to convection (Mosher, 2001). These ABI cloud products will be improved over the current suite, especially if they are computed in conjunction with information from the Hyperspectral Environmental Suite (HES)(Li et al., 2002 a and b), formerly named the Advanced Baseline Sounder (ABS).

2.3 *Sea Surface Temperature (SST)*

The GOES platform allows frequent looks at a given area with the same viewing angle. This scanning feature is exploited to generate improved spatial and temporal coverage of Sea Surface Temperature (SST) from the GOES Imager (Wu et al., 1999). The GOES SST products have many applications, ranging from weather forecasting to fishery management (Seki et al., 2001). The information used to create the SST product will be improved with the ABI due to: higher spatial resolution, more frequent images, more spectral bands, better cloud and aerosol detection and less noisy data.

2.4 *Dust and Volcanic Ash Detection*

The detection of volcanic ash plumes is important for aviation applications (Casadevall, 1992; Davies and Rose, 1998; Hillger and Clark, 2002; Ellrod, 2001). The ABI will improve volcanic ash detection by returning the 12 μm data to the imager (Schmit et al. 2001), but more importantly due to inclusion of the 8.5 μm band.

2.5 *Rainfall Estimations*

Rainfall estimation techniques use data from the GOES Imager; some rely on only the infrared window, for example the auto-estimator (Vicente et al., 1998), and others use more bands, such as the GOES Multispectral Rainfall Algorithm (GMSRA) (Ba and Gruber, 2001). Both types of satellite rainfall estimations will be improved with the ABI data. This is due to the additional bands that will lead to a better cloud-type classification capability. Improved spatial resolution and improved coverage rate will also help. The improved rainfall estimations possible from the ABI data have been investigated by Kuligowski and Im, 2004.

2.6 *Satellite-Derived Wind Fields*

The tracking of atmospheric features (Velden et al., 1997) will be improved using the GOES ABI. The

13.3 μm data will provide better estimates of cloud height for the tracking of atmospheric motions. Currently, the height assignment is one of the greatest sources of error (Nieman et al., 1993). A number of the ABI bands can be used to generate satellite-derived winds at different heights. Satellite-derived winds will be improved with the ABI due to: higher spatial resolution (better edge detection), more frequent images (offers different time intervals), better cloud height detection (with multiple bands), new bands (0.86, 1.38 μm) may allow wind products at different levels, better signal-to-noise ratio and better image navigation/registration.

2.7 *Objective Dvorak Technique*

The GOES Imager is used to determine hurricane location and intensity (Velden et al., 1998 a and b; Goerss et al., 1998; Bosart et al., 2000). The Objective Dvorak Technique is used to monitor the strength of tropical cyclones and relies on the longwave infrared window band (Velden et al., 1998a). The ABI, used in conjunction with the HES, will allow a multi-spectral approach to be further investigated. This product will also be improved due to the improved temporal and spatial resolutions.

2.8 *Biomass Burning/Smoke*

The detection of active fires using primarily the 3.9 μm and the 11 μm bands (Prins et al., 1998) will be improved with the ABI. This is due in part to the improved spatial and temporal resolutions, along with the hotter maximum temperature allowed for the 3.9 μm band. The 0.47 μm band will also detect daytime smoke.

2.9 *Fog Detection*

The bispectral technique for fog detection (Ellrod et al., 1998) is based on differences of the longwave and shortwave IR window brightness temperatures. Using simulated ABI data (derived from 1 km MODerate-resolution Imaging Spectroradiometer (MODIS) data), it has been shown that the fog detection of ABI will be an improvement over the current GOES Imager.

2.10 *Aircraft Icing*

GOES Imagery is used to generate an experimental product that highlights areas of supercooled water clouds that could produce aircraft icing (Ellrod, 1996). This product uses the split window (band 4 minus band 5) temperature difference of greater than 2 K to flag thin cirrus. The addition of the 1.6 and 8.5 μm bands will improve this product.

3. INDIVIDUAL BANDS OF THE PROPOSED ABI

3.1 *0.47 μm or "Blue" Band*

The utility of a band centered at 0.47 μm is well established from many satellites in low-earth orbit, including LANDSAT, SEAWIFS, MODIS and the future VIIRS on NPOESS. A geosynchronous platform is complementary to the polar observers, providing otherwise unknown time-of-day and bi-reflectance data at mesoscale resolution. Blue-band radiometry from GOES-R would provide nearly continuous observations of clouds, dust, haze, smoke, and the health of open waters. Finally, the addition of a blue band (0.47 μm) with a "green band" (0.555 μm) and red (0.64 μm) bands would provide "true" (or natural)-color imagery of the atmosphere and its real time effects on land and sea. Given that the ABI will not have a 0.55μm band, this band will have to be synthesized from other spectral bands.

The blue channel would be particularly valuable for aviation applications. The shorter wavelengths (blue) scatter more off haze and air particles than do the longer wavelengths (red). The current GOES visible channel frequency centered in the red was chosen to minimize scattering by haze in order to see the ground more clearly. Having an additional channel centered near the blue frequencies would greatly improve the detection of haze and enable the calculation of slant range visibility from above. This channel would also have potential applications for air pollution studies, and for improving numerous other products during the day, that rely on obtaining clear sky radiances (i.e. land and sea surface products).

3.2 *0.64 μm or "Red" Band*

A very similar band is on the current GOES Imager. It has many uses, including the diurnal aspects of daytime clouds, fog detection and solar insolation (Diak et al., 1998). The 0.64 μm visible band is also used for: daytime snow and ice cover, detection of severe weather onset detection, low-level cloud drift winds, fog, smoke, volcanic ash, hurricane analysis, and winter storm analysis. Along with the 0.86 μm, an NDVI (Normalized Difference Vegetation Index) will be created.

3.3 *0.86 μm*

The 0.86 μm band is similar to a band on the next generation METEOSAT and would provide synergy with the AVHRR/3. The band is used for daytime clouds, NDVI, fog, aerosols and ocean studies. The band can help in determining vegetation amount, aerosol locations and for ocean/land studies. This enables localized vegetation stress monitoring, fire danger monitoring, fire bur scars and albedo retrieval. Only the GOES perspective can sense the diurnal changes. This may have implication in forecasting forest re-growth patterns. The current GOES visible channel (0.52 - 0.72 μm) does not delineate the burn scars. Other applications include suspended sediment detection (Aquirre-Gomez, 2000). Low-level winds may be derived from time sequences of 0.86 μm images. In some cases, the 0.86 μm band can also be used to help build a false-color imagery.

3.4 *1.38 μm*

The 1.38 μm will help to detect very thin cirrus clouds during the day. This is because the band does not sense into the lower troposphere due to water vapor absorption and thus it provides excellent daytime sensitivity to very thin cirrus. (The 1.38 μm band is centered *within* the atmospheric water vapor absorption region.) These thin clouds may not be detected with any other bands. Contrail detection is important when estimating many surface parameters. There is also interest in the climate change community. When the Total Precipitable Water (TPW) value is too dry (less than approximately 10 mm), then reflectance from the surface minimizes the benefits of this band for thin cirrus detection.

3.5 *1.61 μm*

During the day, the 1.6 μm band can be used for: cloud/snow/ice discrimination, total cloud cover, aviation weather analyses for cloud-top phase (Hutchison 1999), and detecting smoke from low-burn-rate fires. The daytime water/ice cloud delineation is useful for aircraft routing.

3.6 *2.26 μm*

The 2.26 μm is mainly for cloud particle size - detecting particle growth is an indication of cloud growth and intensity of that growth. Although the 1.6 μm band has a larger difference between the imaginary refraction components between the water and ice (Baum et al., 2000), the 2.26 μm band would still be used in this capacity. Other uses of the 2.26 μm band include cloud screening, hot spot detection, and total moisture determinations. For example, the MODIS cloud mask algorithm employs a very similar band (Ackerman et al., 1998). This band is also being considered for the next generation Meteosat imager.

3.7 *3.90 μm*

The shortwave IR window (3.9 μm) band has many uses: fog (Ellrod et al., 1998) and low-cloud discrimination at night, fire identification (Prins et al., 1998), volcanic eruption and ash detection, and daytime reflectivity for snow/ice. This band is based on the current GOES Imager band 2.

3.8 *6.2 μm*

Based on current GOES, and Meteosat Second Generation (MSG/SEVIRI). This band will be used for upper-level tropospheric water vapor tracking; jet stream identification; hurricane track forecasting; mid-latitude storm forecasting; severe weather analysis, rainfall and for estimating upper level moisture.

3.9 *7.0 μm*

Based on current GOES Sounder band 11, and MSG. This band will be used for mid-level tropospheric water vapor tracking, jet stream identification, hurricane track forecasting, mid-latitude storm forecasting, severe weather analysis, and for estimating upper level moisture. Multiple water vapor bands allow for vertical changes to be detected.

3.10 *7.3 μm*

Based on current GOES Sounder band 12. This band will give flow information of the mid/lower levels. It can also identify jet streaks. This band will help with volcanic plumes, given the central wavelength is near 7.3 um.

3.11 *8.5 μm*

The 8.5 μm band, in conjunction with the 11.2 μm band, will enable detection of volcanic dust cloud containing sulfuric acid aerosols (Realmuto et al. 1997; Ackerman and Strabala, 1994).

In addition, the 8.5 μm band can be combined with the 11.2 and 12.3 μm bands to derive cloud phase (Strabala et al. 1994). This determination of the microphysical properties of clouds includes a more accurate and consistent delineation of ice clouds from water clouds during the day or night.

Other uses of the 8.5 μm band include: thin cirrus detection in conjunction with the 11 μm (to improve other products by reducing cloud contamination), a better atmospheric correction in relatively dry atmospheres (to improve SST), and surface properties can be observed in conjunction with the 10.35 μm channel. The MSG carries a similar channel (8.5 to 8.9 μm) as well as MODIS and Global Imager (GLI).

3.12 *9.6 μm*

The addition of a thermal infrared ozone channel (9.7μm) on the GOES-R Imager would provide information both day and night about the real time dynamics of the atmosphere near the tropopause on high spatial and temporal resolutions (Li et. al., 2001). Significant wind shear, turbulence and tropopause folding occur in the middle latitudes, particularly during the baroclinic storms in the spring and fall. The 9.7 μm may give some indications to clear-air turbulence. A 9.6 μm channel on ABI would also complement a similar channel on MSG, as part of a global observing system.

3.13 *10.35 μm*

The 10.35 μm band will help to derive low-level moisture, cloud particle size and surface properties. Chung et al. (2000) showed how the 10 - 11 μm region is important for determining particle sizes of ice-clouds.

3.14 *11.2 μm*

The longwave infrared window (11.2 μm) band will provide day/night cloud analyses for general forecasting and broadcasting applications, precipitation estimates (Vicente et al., 1998), severe weather analyses, cloud drift winds (Velden et al. 1998a), hurricane strength (Velden et al. 1998b) and track analyses, cloud top heights, volcanic ash detection (Prata 1989), fog detection in multi-band products (Lee et al. 1997), winter storms, and cloud phase/particle size estimates in multi-band products.

3.15 *12.3 μm*

The 12.3 μm band will offer nearly continuous cloud monitoring for numerous applications, low-level moisture determinations, volcanic ash identification detection (Davies and Rose 1998), Sea Surface Temperature measurements (Wu et al. 1999), and cloud particle size (in multi-band products). It has been shown that mid-level dust amounts (from the Saharan Air Layer) may be useful in determining hurricane intensification in the Atlantic basin.

3.16 *13.3 μm*

The 13.3 μm band will be used for cloud top height assignments for cloud-drift winds, cloud products for ASOS supplement (Schreiner et al. 1993; Wylie and Menzel 1999), tropopause delineation, and estimating cloud opacity. These cloud products will be further improved by combining the data with high-spectral resolution sounder data from HES.

Table 1. Summary of the bands on the current GOES Imagers from Hillger et al. (2003).

Current GOES Imager Band	Wavelength Range (μm)	Central Wavelength (μm)	Meteorological Objective
1	0.55 to 0.75	0.65	Cloud cover and surface features during the day
2	3.8 to 4.0	3.9	Low cloud/fog and fire detection
3	6.5 to 7.0 5.8 to 7.3	6.75 **(GOES-8/11)** 6.48 **(GOES-12)**	Upper-level water vapor
4	10.2 to 11.2	10.7	Surface or cloud-top temperature
5	11.5 to 12.5	12.0 **(GOES-8/11)**	Surface/cloud-top temperature and low-level water vapor
6	12.9 to 13.7	13.3 **(GOES-12)**	CO_2 band: Cloud detection

Table 2. Summary of the bands on the future GOES Imagers (ABI).

Future GOES Imager (ABI) Band	Wavelength Range (μm)	Central Wavelength (μm)	Objective
1	0.45-0.49	0.47	Daytime aerosol-over-land, Color imagery
2	0.59-0.69	0.64	Daytime clouds fog, insolation, winds
3	0.84-0.88	0.86	Daytime vegetation & aerosol-over-water, winds
4	1.365-1.395	1.38	Daytime cirrus cloud
5	1.58-1.64	1.61	Daytime cloud water, snow
6	2.235 - 2.285	2.26	Day land/cloud properties, particle size, vegetation
7	3.80-4.00	3.90	Sfc. & cloud/fog at night, fire
8	5.77-6.6	6.19	High-level atmospheric water vapor, winds, rainfall
9	6.75-7.15	6.95	Mid-level atmospheric water vapor, winds, rainfall
10	7.24-7.44	7.34	Lower-level water vapor, winds & SO_2
11	8.3-8.7	8.5	Total water for stability, cloud phase, dust, SO_2
12	9.42-9.8	9.61	Total ozone, turbulence, winds
13	10.1-10.6	10.35	Sfc. & cloud
14	10.8-11.6	11.2	Total water for SST, clouds, rainfall
15	11.8-12.8	12.3	Total water & ash, SST
16	13.0-13.6	13.3	Air temp & cloud heights and amounts

Table 3. A comparison of the current and future imagers.

Parameter	Current GOES Imager	Future GOES Imager	Comments
Visible bands	1	3	ABI will be either 0.5 or 1 km
Near IR bands	0	3	ABI will be approximately 1 km
Infrared bands	4	10	ABI will be approximately 2 km
Coverage Rate	25 minutes for full disk	Approximately 5 minutes for full disk	Approximately five times faster

4. BAND SELECTION AND RECENT CHANGES

Each ABI band selection has been chosen by building upon the experience of heritage instruments and being aware of other sensors that will be available in the GOES-R era, while meeting the stated user requirements. There have been several recent developments and changes. For example, while other bands were considered the ABI will be a 16 band instrument. Of these bands, several were spectrally modified to be slightly different.

For example, the shortwave side of the 6.15 µm (wide) water vapor band was shortened to be more consistent with GOES-12+ Imagers and MSG. This band was shifted from 5.7 – 6.6 µm to 5.77 to 6.6 µm. The center frequency is now 6.19 µm. The mean brightness temperature difference due to this change is approximately 0.2K.The other two water vapor bands were also spectrally shifted to allow for a cleaner SO_2 measurement. The water vapor mission will still be accomplished. By slightly shifting both of these, a cleaner "on" and "off" SO_2 measurement can be accomplished. Spectral absorption by SO_2 gas (Figure 4) emitted from volcanoes occurs in a number of discrete bands centered near 4.0 µm, 7.3 µm, and 8.6 µm. These bands tend to be quite narrow. Of course the 8.5 µm will also be used, but having this pair might help in the height assignment, give more upper-level information and may be used for more quality control. So the 7.4 µm (7.3 to 7.5 µm) band was shifted to a 7.34 µm band (7.24 to 7.44 µm) and the 7.0 µm band (6.8 to 7.2 µm) was shifted to a 6.95 µm (6.75 to 7.15 µm). The effects of shifting the spectral responses have been studied with both forward calculations and by convolving ABI SRFs with AIRS measurements. The shifts in brightness temperature are on the order of 1 degree. For more sample ABI-like spectral images, see *http://cimss.ssec.wisc.edu/goes/abi/airs_broadcast/aniairs.html*. These images are built from AIRS data received via direct broadcast at the Space Science and Engineering Center (SSEC) in Madison, WI.

The 50% response points of the 9.7 µm band were widened to 9.42 - 9.8 µm. The center wavelength is 9.61 µm (Figure 5). The spectral tolerances are still +/- 0.02 and +/- 0.03 µm for the lower and higher wavelength sides, respectively. For more information on the trade-offs between low and high spectral resolution GOES ozone retrievals, see Schmidt et al, 2004.

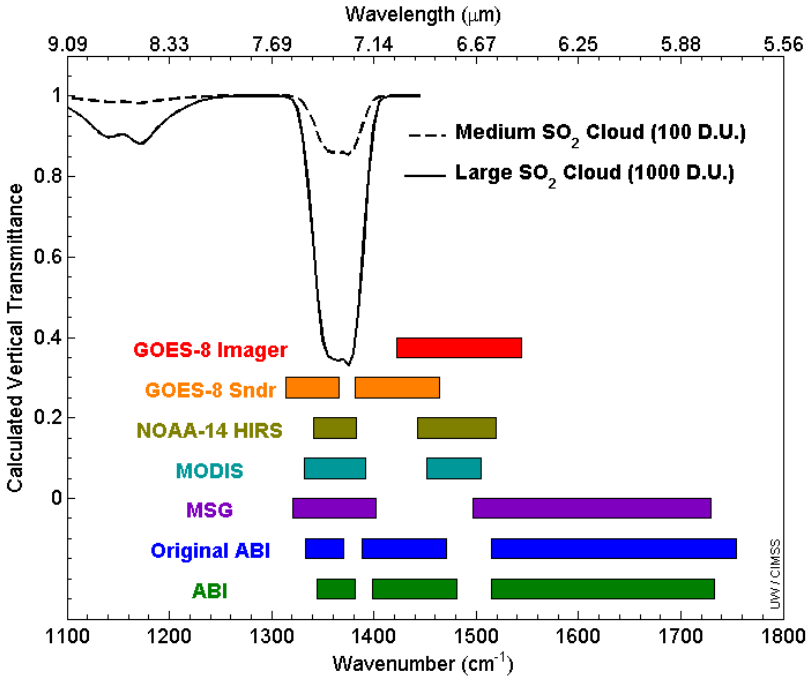

Figure 4. Spectral widths of several spectral bands near a SO_2 signature (from F. Prata of CSIRO).

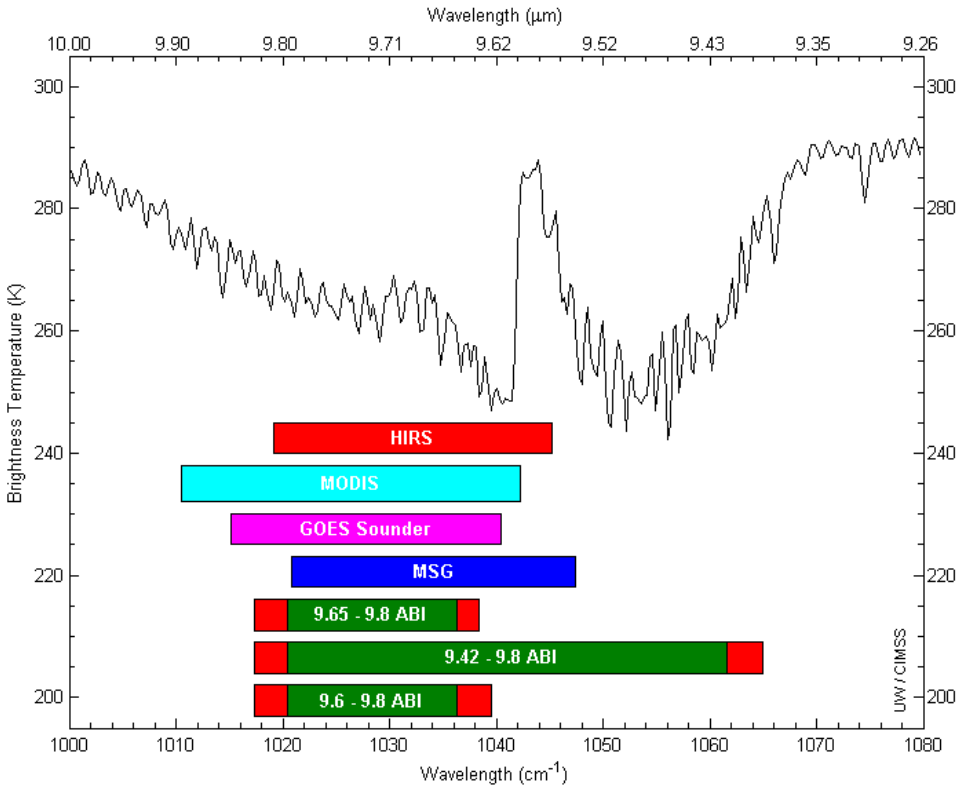

Figure 5. Spectral widths of the previous (narrow) and new (wide) ozone band on the ABI. The spectral tolerances are shown for the ABI. Spectral bandwidths from other sensors and an earth-emitted spectra are also plotted.

5. SUMMARY

The ABI represents an exciting expansion in geostationary remote sensing capabilities. The ABI addresses the needs of the National Weather Service (and others) by increasing spatial resolution (to better depict a wider range of phenomena), by scanning faster (to improve temporal sampling and to scan additional regions) and by adding spectral bands (to enable new and improved products). Every product that is being produced from the current GOES Imager will be improved with data from the ABI.

Of course the ABI will not be operating alone. Where appropriate, products will be produced in concert with the GOES-R high-spectral resolution sounder. It has been shown that several products can be improved when using high spatial resolution imager data with co-located high-spectral resolution measurements (Li et al 2003a, Li et al 2003b). In the preceding case, MODIS/AIRS was used to simulate the ABI/HES synergy. Also, the GOES system complements the polar systems and the entire Global Observing System (GOS).

The next generation METEOSAT (launched in 2002) has 12 bands, including two water vapor bands centered at 6.2 and 7.3 µm (Schmetz et al., 1998; Schmetz et al., 2002, Woick et al., 1997).

ACKNOWLEDGMENTS: The authors would like to thank the host of CIMSS, NOAA NESDIS and other scientists that contributed to the ABI band selection.

REFERENCES

Ackerman, S. A., and H. Chung, 1992: Radiative effects of airborne dust on regional energy budgets at the top of the atmosphere. *J. Atmos. Sci.*, 31, 223–236.

Ackerman, S. and K. I. Strabala, 1994: Satellite remote sensing of H_2SO_4 aerosol using the 8 to 12 µm window region: Application to Mount Pinatubo. *J. Geo. Res.*, **99**, 18,639-18,649.

Ackerman, S. A., 1996: Global satellite observations of negative brightness temperature differences between 11 and 6.7 µm. *J. Atmos. Sci.,* 53, 2803–2812.

Ackerman, S. A., K. I. Strabala, W. P. Menzel, R. A. Frey, C. C. Moeller, and L. E. Gumley, 1998: Discriminating clear sky from clouds with MODIS. *J. Geophys. Res*., 103, 32141-32157.

Aquirre-Gomez, R., 2000: Detection of total suspended sediments in the North Sea using AVHRR and ship data. *Int. J. Remote Sensing*, 21, 1583-1596.

Ba, M., and A. Gruber, 2001: GOES Multispectral Rainfall Algorithm (GMSRA). *J. Appl. Meteor*., Vol. 40, No. 8, 1500–1514.

Barton, I. J., A. J. Prata, I. G. Watterson, and S. A. Young, 1992: Identification of the Mount Hudson volcanic cloud over SE Australia. *Geophys. Res. Lett.,* 19, 1211-1214.

Bayler, G. M., R. M. Aune, and W. H. Raymond, 2001: NWP cloud initialization using GOES sounder data and improved modeling of non-precipitating clouds. *Mon. Wea. Rev*., 128, 3911-3920.

Baum, B. A., P. F. Soulen, K. I. Strabala, M. D. King, S. A. Ackerman,W. P. Menzel, and P. Yang, 2000: Remote sensing of cloud properties using MODIS Airborne Simulator imagery during SUCCESS. II. Cloud thermodynamic phase. J. Geophys. Res., 105, 11,781-11,792.

Bosart, L. F., C. S. Velden, W. E. Bracken, J. Molinari, and P. G. Black, 2000: Environmental influences on the rapid intensification of Hurricane Opal (1995) over the Gulf of Mexico. *Mon. Wea. Rev.,* 128, 322–352.

Casadevall, T.J., 1992: Volcanic hazards and aviation safety: Lessons of the past decade,
FAA Aviation Safety Journal, 2 (3), 1-11.

Chung S., S. Ackerman, and P. F. van Delst, 2000: Model calculations and interferometer measurements of ice-cloud characteristics. *J. Appl. Met*., 39, 634-644.

Davies, M. A., and W. I. Rose, 1998: Evaluating GOES imagery for volcanic cloud observations at the Soufriere Hills volcano, Montserrat. *Amer. Geophys. Union Proc*., in press.

Diak, G. R., M. C. Anderson, W. L. Bland, J. M. Norman, J. M. Mecikalski, and R. A. Aune, 1998: Agricultural management decision aids driven by real time satellite data. *Bull. Amer. Meteor. Soc*., 79, 1345-1355.

Dostalek, J. F., J. F. Weaver, J. F. W. Purdom, K. Y. Winston, 1997: PICTURE OF THE QUARTER: Nighttime Detection of Low-Level Thunderstorm Outflow Using a GOES Multispectral Image Product. Weather and Forecasting: Vol. 12, No. 4, 947–950.

Ellrod, G. P., 1996: The use of GOES-8 multispectral imagery for the detection of aircraft icing regions. Preprint Volume, *8th Conf. on Satellite Meteorology and Oceanography*, Atlanta, Georgia, Amer. Meteor. Soc., Boston, 168-171.

Ellrod, G. P., R. V. Achutuni, J. M. Daniels, E. M. Prins, and J. P. Nelson III, 1998: An assessment of GOES-8 Imager data quality, *Bull. Amer. Meteor. Soc.*, 79, 2509-2526.

Ellrod, G. P., 2001: Loss of the 12.0 mm "split window" band on GOES-M: Impacts on volcanic ash detection. *11th Conference on Satellite Meteorology and Oceanography*, 15—18 October, Madison, WI.

Frey, R. A., B. A. Baum, W. P. Menzel, S. A. Ackerman, C. C. Moeller, and J. D. Spinhime, 1999: A comparison of cloud top heights computed from airborne LIDAR and MAS radiance data using CO_2-slicing, *J. Geophys. Res.,* 104, 24,547-24,555.

Goerss, J. S., C. S. Velden, and J. D. Hawkins, 1998: The impact of multispectral GOES-8 wind information on Atlantic Tropical Cyclone track forecasts in 1995. Part II: NOGAPS Forecasts. *Mon. Wea. Rev*, 126, 1219–1227.

Gurka J. J., and G. J. Dittberner, 2001: The next generation GOES instruments: status and potential impact. Preprint Volume. 5th Symposium on Integrated Observing Systems. 14-18 January, Albuquerque, NM., Amer. Meteor. Soc., Boston.

Hayden, C. M., G. S. Wade, and T. J. Schmit, 1996: Derived product imagery from GOES-8. *J. Appl. Meteor*., 35, 153-162.

Hillger, D. W., 1996: Meteorological features from principal component image transformation of GOES imagery, Proceedings, *GOES-8 and Beyond*, Intl. Soc. Optical Engineering, Denver, Colorado, 111-121.

Hillger, D. W., and J. Clark, 2002: Principal Component Image Analysis of MODIS for Volcanic Ash, Part-2: Simulation of Current GOES and GOES-M Imagers, *J. Appl. Meteor*., Vol. 41, No. 10, 1003–1010.

Hillger, D. W., T. J. Schmit, and J. M. Daniels, 2003: Imager and Sounder Radiance and Product Validations for the GOES-12 Science Test, NOAA Technical Report 115, U.S. Department of Commerce, Washington, DC.

Hutchison, K. D., 1999: Application of AVHRR/3 imagery for improved detection of thin cirrus clouds and specification of cloud-top phase. *J. Atmos. Oceanic Tech*., 16, 1885-1899.

Kim, D., and S. G. Benjamin, 2000: Assimilation of cloud-top pressure derived from GOES sounder data into MAPS/RUC. Preprints, *10th Conf. on Satellite Meteorology and Oceanography*, Long Beach, CA, Amer. Meteor. Soc., 110-113.

Kuligowski, R. J. and S. Im, 2004: Potential Impact Of Proposed Advanced Baseline Imager (ABI) Channels On Satellite Precipitation Estimation, 20th International Conference on Interactive Information and Processing Systems (IIPS) for Meteorology, Oceanography, and Hydrology, Seattle, WA.

Lee, T. F., F. J. Turk, K. Richardson, 1997: Stratus and Fog Products Using GOES-8–9 3.9-m Data. *Wea. Forecasting,* Vol. 12, No. 3, 664–677.

Li, J., C. C. Schmidt, J. P. Nelson III, T. J. Schmit, and W. P. Menzel, 2001: Estimation of total atmospheric ozone from GOES sounder radiances with high temporal resolution. *J. Atmos. Oceanic Technol.,* 18, 157-168.

Li, J., T. J. Schmit, and W. P. Menzel, 2002, Advanced Baseline Sounder (ABS) for future Geostationary Operational Environmental Satellites (GOES-R and beyond)", Proceeding of SPIE, *Applications with Weather Satellites*, Hangzhou, China.

Li, J., W. P. Menzel, Z. Yang, R. A. Frey, S. A. Ackerman, 2002: High-spectral resolution surface and cloud type classification from MODIS multi-spectral band measurements, submitted to *J. Appl. Meteor.,* Vol. 42, No. 2, 204–226.

Li, J., W. P. Menzel, F. Sun, T. J. Schmit, and J. Gurka, 2003a: AIRS sub-pixel cloud characterization using MODIS cloud products*, J. Appl. Meteorol.* (submitted).

Li, J., W. P. Menzel, W. Zhang, F. Sun, T. J. Schmit, J. Gurka, and E. Weisz, 2003b: Synergistic
use of MODIS and AIRS in a variational retrieval of cloud parameters, *J. Appl. Meteorol,* (submitted).

Menzel, W. P., and J. F. W. Purdom, 1994: Introducing GOES-I: The first of a new generation of geostationary operational environmental satellites, *Bull. Amer. Meteor. Soc.*, 75, 757-781.

Moeller, C. C., S. A. Ackerman, K. I. Strabala, W. P. Menzel, and W. L. Smith, 1996: Negative 11 micron minus 12 micron brightness temperature differences: a second look, *8th Conference on Satellite Meteorology and Oceanography*, Atlanta, GA, Amer. Meteor. Soc. 313-316.

Moody J. L., A. J. Wimmers, and J. C. Davenport, 1999: Remotely sensed specific humidity: development of a derived product from the GOES Imager channel 3, G*eo. Phys. Let.*, 26, 59-62.

Mosher, F. R., 2001: A Satellite Diagnostic of Global Convection. *11th Conference on Satellite Meteorology and Oceanography*, 15—18 October, Madison, WI.

Nieman, S. J., J. Schmetz, and W. P. Menzel, 1993: A comparison of several techniques to assign heights to cloud tracers. *J. Appl. Meteor*., 32, 1559-1568.

Prata, A. J., 1989: Observations of volcanic ash clouds in the 10-12 μm window using AVHRR/2 data. *Int. J. Remote Sens*., 10, 751-761.

Prins, E. M., J. M. Feltz, W. P. Menzel, and D. E. Ward, 1998: An overview of GOES-8 diurnal fire and smoke results for SCAR-B and 1995 fire season in South America, *J. Geophysical Res*., 103, 31821-31835.

Realmuto, V. J., A. J. Sutton, T. Elias, 1997: Multispectral thermal infrared mapping of sulfur dioxide plumes: A case study from the East Rift Zone of Kilauea Volcano, Hawaii, *J. Geophys. Res*., 102, 15,057-15,072.

Schmidt, C. J. Li, F. Sun, 2004: Simulation and Comparison Between GIFTS, ABI, And GOES I-M Sounder Ozone Estimates And Applications To HES, 20th International Conference on Interactive Information and Processing Systems (IIPS) for Meteorology, Oceanography, and Hydrology, Seattle, WA.

Schmit, T. J., E. M. Prins, A. J. Schreiner, and J. J. Gurka, 2001: Introducing the GOES-M imager. *Nat. Wea. Assoc. Digest*. Volume 25 Nos 3,4.

Schreiner, A. J., D. A. Unger, W. P. Menzel, G. P. Ellrod, K. I. Strabala, and J. L. Pellett, 1993: A comparison of ground and satellite observations of cloud cover. *Bull. Amer. Meteor. Soc*., 74, 1851-1861.

Schreiner, A. J., T. J. Schmit, and W. P. Menzel, 2001: Trends and observations of clouds based on GOES sounder data. *J. Geophysical Res. –Atmospheres,* 106, 20,349-20,363.

Seki, M. P., J. J. Polovina, R. E. Brainard, R. R. Bidgare, C. L. Leonard, and D. G. Foley, 2001: Biological enchancement at cyclonic eddies tracked with GOES thermal imagery in Hawaiian waters. *Geophysical Research Letters,* 28 (8), 1583.

Schmetz, J., H. Woick, S. Tjemkes, and J. Rattenborg, 1998: From Meteosat to Meteosat Second Generation, In Proceedings of the Ninth Conference on Satellite Meteorology and Oceanography, Paris, France, Amer. Meteor. Soc., 335-338.

Schmetz, J., P. Pili, S. Tjemkes, D. Just, J. Kerkmann, S. Rota, A. Ratier, 2002: An Introduction to Meteosat Second Generation (MSG). *Bull. Amer. Meteor. Soc.*, Vol. 83, No. 7, 977–992.

Soden, B. J., and F. P. Bretherton, 1993: Upper tropospheric relative humidity from the GOES 6.7 μm channel: Method and climatology for July 1987. *J. Geophys. Res.,* 98, 16669-16688.

Strabala, K. I., S. A. Ackerman, and W. P. Menzel, 1994: Cloud properties inferred from 8-12 μm data. *J. Appl. Meteor*, 33, 212-229.

Velden, C. S., C. M. Hayden, S. J. Nieman, W. P. Menzel, S. Wanzong, and J. S. Goerss, 1997: Upper-tropospheric winds derived from geostationary satellite water vapor observations. *Bull. Amer. Meteor. Soc.*, 78 (2), 173-173.

Velden, C. S., T. L. Olander, and R. M. Zehr, 1998a: Development of an objective scheme to estimate tropical cyclone intensity from digital geostationary satellite infrared imagery. *Wea. Forecasting*, 13 (1), 172–186.

Velden, C. S., T. L. Olander, and S. Wanzong, 1998b: The impact of multispectral GOES-8 wind information on Atlantic tropical cyclone track forecasts in 1995. Part I: dataset methodology, description, and case analysis, *Mon. Wea. Rev.*, 126(5), 1202–1218.

Vicente, G. A., R. A. Scofield, and W. P. Menzel, 1998: The operational GOES infrared rainfall estimation technique, *Bull. Amer. Meteor. Soc.*, Vol. 79 (9), 1883–1898.

Weldon, R. B, and S. J. Holmes, 1991: Water vapor imagery -- interpretation and applications to weather analysis and forecasting, NOAA Technical Report NESDIS 57.

Woick, H., J. Schmetz, and S. Tjemkes, 1997: An introduction to Meteosat Second Generation imagery and products, *1997 Meteorological Data Users' Conference*, Brussels, Belgium.

Wu, Xiangqian, W. P. Menzel, and Gary S. Wade, 1999: Estimation of sea surface temperatures using GOES-8/9 radiance measurements. *Bull. Amer. Meteor. Soc.*, 80 (6), 1127-1138.

Wylie, D. P., W. P. Menzel, H. M. Woolf, and K. I. Strabala, 1994: Four years of global cirrus cloud statistics using HIRS. *J. Climate*, 7, 1972-1986.

Wylie, D. P., and P. H. Wang, 1997: Comparison of cloud frequency data for the High Resolution Infrared Radiometer Sounder and the Stratospheric Aerosol and Gas Experiment II. *J. of Geophys. Res.*, 102 (29), 29,893-29,900.

Wylie, D. P., and W. P. Menzel, 1999: Eight years of high cloud statistics using HIRS. *J. Climate*, 12, 170-184.